

Petrology and tectonic history of the Green Bay Schist, Portmore, St. Catherine Parish, Jamaica

RICHARD N. ABBOTT, JR.¹, DAVID P. WEST, JR.², BETSY R. BANDY³
AND RYAN J. MCALEER⁴

¹Department of Geology, Appalachian State University, Boone, NC 28608. E-mail: abbottrn@appstate.edu

²Department of Geology, Middlebury College, Middlebury, VT 05753. E-mail: dwest@middlebury.edu

³Ministry of Science, Technology, Energy and Mining, Kingston, Jamaica. E-mail: bbandy@mstem.gov.jm

⁴U.S. Geological Survey, MS 926 National Center, Reston, VA 20192. E-mail: rmcaleer@usgs.gov

ABSTRACT. There are three occurrences of medium- to high-grade metamorphic rocks in Jamaica: amphibolite facies Westphalia Schist, blueschist/greenschist facies Mt. Hibernia Schist, and the hitherto poorly characterized amphibolite facies Green Bay Schist. New trace element data and thermodynamic calculations show that Green Bay Schist is closely related to Westphalia Schist. The protoliths for both are very similar (basalt-andesitic basalt, C-MORB), consistent with a subducted ocean-ridge tectonic environment, hence arc-related. The protolith for Mt. Hibernia Schist is quite different (basalt, P-MORB), related to the Caribbean Large Igneous Province. Whereas the P-T-t paths for Green Bay Schist and Westphalia Schist prior to the middle Campanian (>78 Ma) are inferred to be similar, the late Campanian, Maastrichtian and Cenozoic P-T-t paths are very different. New ⁴⁰Ar/³⁹Ar age determinations show the following: (1) While the difference in the late Campanian and Maastrichtian remains problematic, (2) the difference in the Cenozoic clearly reflects the location relative to the NW-trending, NE-dipping Wagwater Fault: Westphalia Schist to the NE (hanging wall); Green Bay Schist to the SW (foot wall). The Cenozoic P-T-t paths are complementary, and consistent with the behavior of the Wagwater Fault: 65-50 Ma, normal motion (transtension); 50-10 Ma, inactive (quiescent); 10 Ma-present, reverse motion (transpression).

Keywords: Caribbean, Jamaica, tectonics, metamorphism, thermochronology.

1. INTRODUCTION

Two small exposures of metamorphic rock at Green Bay, southwest of Kingston, Jamaica, were the subject of a heated debate in the 1940s and early 1950s – a debate concerning, among other things, an eccentric (pre-plate tectonic) theory of mountain building (see discussion in [Donovan, 2008, 2010](#)). The controversy was effectively resolved with [Chubb's \(1954; Donovan, 2010\)](#) observations and mapping of the site. Draper visited the site c. 1976 in conjunction with his dissertation ([Draper, 1979](#); and see [Draper, 1987](#)), but since then, until our recent visit in 2013, Green Bay has been closed to the public by the Jamaican Defense Force (JDF), used the site intermittently over the years as an artillery range. The possibility of unexploded ordinance has been very effective in dissuading would-be trespassers, and maintaining the long hiatus between Draper's (c. 1976) field work and our visit. [Draper \(1979, 1987\)](#) reported whole-rock chemical analyses for major elements in one rock sample and chemical analyses of two amphiboles from Green Bay Schist. [Kemp \(1971\)](#) and then [Draper \(1979, 1987\)](#) were among the first to speculate that Green Bay Schist may be equivalent to the amphibolite facies Westphalia Schist, approximately 30 km to the east in the Blue Mountains. The simple objective of this study is to test

[Kemp's \(1971\)](#) and [Draper's \(1979, 1987\)](#) hypothesis by using modern geochemistry and petrology to compare Green Bay Schist with well-studied metamorphic rocks in the Blue Mountains ([West et al., 2014](#)). To this end, we examine major-element mineral chemistry to estimate the P-T conditions, whole-rock major-element and trace-element chemistry to characterize the protolith and tectonic provenance, and ⁴⁰Ar/³⁹Ar data to constrain cooling ages.

With permission from the JDF and an armed military escort we visited the site for approximately 4 hours, 9 August 2013, for the purpose of collecting samples for petrographic and geochemical analysis. The party included two of the authors (RNA, BRB), four JDF soldiers, Prof. Simon F. Mitchell (University of the West Indies) and two of his students. Prof. Mitchell and his students took advantage of the opportunity to verify upper Eocene to Miocene limestone stratigraphy mapped by [Chubb \(1954\)](#).

Abbreviations for minerals and mineral components conform to [Kretz \(1983\)](#), as updated by [Whitney and Evans \(2010\)](#), except for abbreviations for components used in thermodynamic calculations (figure 9, explained in table 5). In the convention ([Kretz, 1983](#); [Whitney and Evans, 2010](#)), abbreviations for minerals are capitalized; abbreviations

for components are not capitalized, e.g., “Ab” standards for a plagioclase with “ab” content greater than 90%. K-Ar ages reported from Lewis et al. (1973) are corrected for currently accepted argon decay constants (Steiger and Jäger, 1977). Absolute stratigraphic ages and Geologic Time Scale nomenclature are consistent with Gradstein et al. (2012). In the present context, early/lower, middle, late/upper subdivisions of the Cenozoic epochs are informal, hence not capitalized.

2. GEOLOGY

2.1. General tectonic framework.

Jamaica is the third largest of the islands of the Greater Antilles (Figure 1A, Puerto Rico, 4th largest, not shown). The island is cut by the E-W trending left-lateral transform system of the Enriquillo-Plantain Garden Fault. As such, the island straddles the boundary between the Caribbean Plate and the Gonave Microplate (Figure 1A). The Blue Mountains in eastern Jamaica (>2200 m)

owe their relief to middle Miocene–present uplift in response to NE-SW compression at a prominent right-step, left-lateral restraining bend along the Plantain Garden segment of the transform boundary (Mann et al., 1985; Dominguez-Gonzalez et al., 2015).

The basement of Jamaica was formed as part of a Cretaceous (or earlier) volcanic island arc. The basement consists of a diverse assemblage of unmetamorphosed and metamorphosed volcanic, sedimentary and plutonic rocks (e.g., Robinson, 1994; Mitchell, 2003, 2006). The arc-related rocks are unconformably overlain by Cenozoic strata. The basement is now exposed in a number of inliers (Figure 1B), where locally the younger strata have been eroded away. The unconformity at the base of the oldest Cenozoic strata, redbeds of the Wagwater Formation, indicates that at least some basement was exposed at the surface by the end of the Cretaceous or by early Paleocene (~66 Ma).

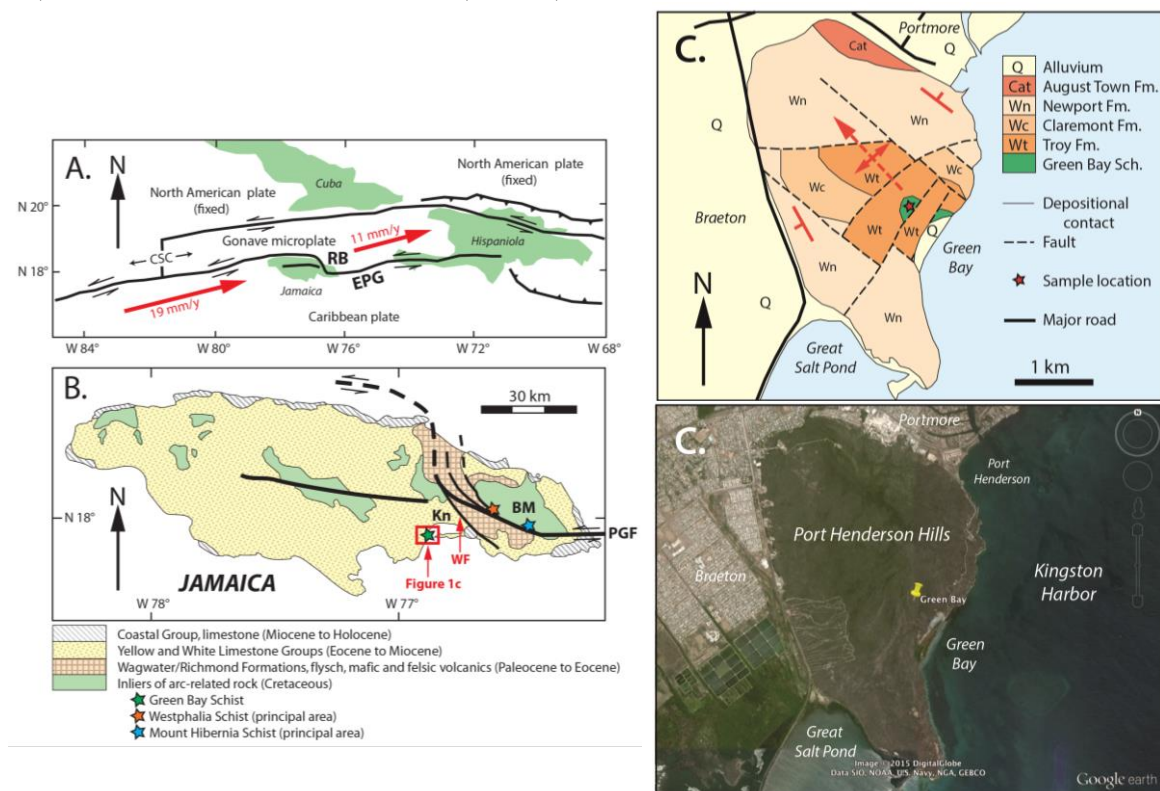


Figure 1. Regional geology. A. Plate tectonic setting of Jamaica. The red vectors (DeMets and Wiggins-Grandison, 2007) show the motions of the Caribbean Plate and Gonave Microplate relative to the North American Plate. CSC = Cayman spreading center, EPG = Enriquillo - Plantain Garden Fault, and RB = restraining bend. B. Simplified geologic map of Jamaica, after Mitchell (2013). PGF = Plantain Garden Fault, BM = Blue Mountains Inlier, WF = Wagwater Fault, Kn = Kingston. Red box is the study area. C. Geologic map of Green Bay (after Mitchell, 2015) and Google Earth image (©2015 Google Inc.) of the same area depicted in the geologic map. The map unit identified as Wt (upper Eocene, Troy Formation) also includes one very small area of Cavalier Formation. The map unit identified as Wc (Eocene, Claremont Formation) includes small areas of Swanswick and Somerset Formations. The map unit identified as Wn (Miocene, Newport Formation) includes small areas of Walderston Formation. The August Town Formation is Miocene-Pliocene (James-Williamson et al., 2014).

The largest of the inliers is the Blue Mountains Inlier in eastern Jamaica (**Figure 1B**). Near the SW margin of the Blue Mountains Inlier, greenschist-blueschist facies Mt. Hibernia Schist and amphibolite facies Westphalia Schist (**Draper, 1979, 1986, 1987; Abbott et al., 1996, 2003, 2011; Abbott and Bandy, 2008**) have been uplifted on the NE side of the restraining bend (**Mann et al., 1985; 2007; Dominguez-Gonzalez et al., 2015**) along the Plantain Garden-Blue Mountains Fault System (**Figure 1A, B**). K-Ar ages on hornblende from the Westphalia Schist give a cooling age of ~77 Ma, while biotite from the same rock gives ages of 50 and 54 Ma (**Lewis et al., 1973**). Recently determined whole-rock $^{40}\text{Ar}/^{39}\text{Ar}$ ages of 74 and 77 Ma for Mt. Hibernia Schist (**Abbott et al., 2011; West et al., 2014**) are consistent with the older K-Ar hornblende age. Whereas, recently determined whole-rock and K-feldspar $^{40}\text{Ar}/^{39}\text{Ar}$ cooling ages for Westphalia Schist (**Abbott et al., 2011; West et al., 2014**) are consistent with the younger K-Ar biotite ages. $^{40}\text{Ar}/^{39}\text{Ar}$ determinations for Westphalia Schist give an early Eocene whole-rock cooling age of 53 Ma and a middle Paleocene K-feldspar cooling age of ~60 Ma (**Abbott et al., 2011; West et al., 2014**). The younger ages (50-60 Ma) are more recent than the unconformity at the base of the Wagwater Formation, and relate to low-grade upper zeolite facies burial metamorphism (**Abbott et al., 2013; West et al., 2014**).

2.2. Four tectonic stages.

The geology of Jamaica unfolded in four tectonic stages (**Robinson, 1994; Mann and Burke, 1990; Draper, 2008**), as follows (**Figure 2**):

(1) Island arc and convergent plate boundary tectonics: Early Cretaceous–early Paleocene formation of the original Caribbean Large Igneous Province (CLIP, 86-92 Ma, **Hastie et al., 2008; West et al., 2014**) and volcanic island arc (>90 Ma, **Hastie et al., 2010**), followed by exhumation between ~80 Ma and ~65 Ma (**West et al., 2014**).

(2) Transensional subsidence: Early Paleocene to early Eocene redbeds and volcanic rocks of the Wagwater and Richmond Formations occupy a NW-trending half-graben formed during transensional tectonics (**Figure 1B**). East-dipping listric normal faults along the western margin of the half-graben (Wagwater Fault, **Figure 1B**) were active during this time, and also affected the interior of the basin (**Draper, 2008**). The Wagwater Fault is shown schematically in **Figure 2**. The combined thickness of the Wagwater and Richmond Formations is at least 6.8 km (**Mann and Burke, 1990**). The strata were affected by burial metamorphism during this time (**Abbott et al., 2013; West et al., 2014**).

(3) Quiescence: Middle Eocene deep-water limestone overlies the Wagwater and Richmond Formations. Elsewhere in Jamaica, the age of the oldest limestone varies from early or middle Eocene in central Jamaica (**Robinson, 1994; Draper, 2008; Mitchell, 2013**) to late Paleocene or early Eocene in eastern Jamaica (**Mann and Burke, 1990; Robinson, 1997**). In the vicinity of the Wagwater and Richmond Formations, the early deep-water limestone is overlain by upper Eocene to Miocene mostly shallow-water limestone. For the purpose of this study, it is assumed that the transition from the Wagwater-Richmond sequence to limestone deposition (Yellow and White Limestone Groups) took place in the early Eocene, at ~50 Ma (**Mann and Burke, 1990**, corrected for modern PICKS, **Gradstein et al., 2012**). However, it should be noted that middle Eocene olistostromes in the lower part of the White Limestone Group (**Robinson, 1967; Mitchell, 2004**) suggest that movement on the Wagwater Fault may have continued into the middle or late Eocene. Otherwise, the Yellow and White Limestone Groups represent a relatively quiet time of diminished fault activity. **Draper (2008)** suggested that the limestone is related to epeirogenic subsidence in response to lithospheric cooling.

(4) Transpressional uplift: Late Miocene (~10 Ma, **Draper, 2008**) to Pleistocene carbonate reef deposits, now raised above sealevel, are related to ongoing transpressional uplift. Earlier normal faults (stage 2) were reactivated as reverse faults (**Dominguez-Gonzalez et al., 2015**).

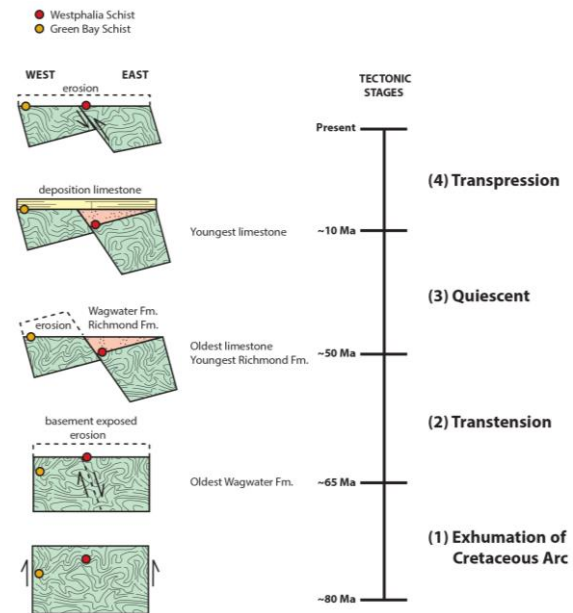


Figure 2. Four tectonic stages. Schematic SW-NE cross sections across the Wagwater Fault, which forms the western margin of the Wagwater and Richmond Formations.

2.3. Green Bay Inlier.

This small inlier is actually comprised of two parts (**Figure 1C**), both of which are exposed along the axis of a NW-plunging anticline, which itself is dissected by numerous faults (**Mitchell, 2015**). At Green Bay, redbeds of the Wagwater and Richmond Formations (stage 2, **Figure 2**) are missing, such that platform limestone (upper Eocene–Miocene, stage 3, **Figure 2**) rests nonconformably on the Green Bay Schist (**Chubb, 1954; Donovan, 2008, 2010; Mitchell, 2015**). When movement on the Wagwater Fault was normal (stage 2, **Figure 2**), rocks in the Green Bay Inlier were in the footwall, west of the depositional basin of the Wagwater and Richmond Formations. The stratigraphy only indicates that Green Bay Schist was exposed at the surface at the commencement of the deposition of the platform limestone (~50 Ma, stage 3, **Figure 2**). The anticline and faulting that expose the Green Bay Inlier are interpreted as a local manifestation of late, regional NE-SW compression (stage 4, **Figure 2**), related to the uplift of the Blue Mountains (**Draper, 2008**).

3. METHODS

3.1. Sampling.

Sampling was informed by **Chubb's (1954)** original geologic map, here updated (**Figure 1C**) according to **Mitchell (2015)**, with a Google Earth (©2015 Google Inc.) satellite image of the same area. For the purpose of chemical analyses of trace elements, the sea-cliff exposure (**Donovan, 2010**) was avoided to minimize any influence of weathering and contamination by sea water. Samples were chipped from six fresh boulders (JAM-13-1a, b, c, d, e, f) in the talus below the principal exposure. The sample location is indicated in **Figure 1C**. Polished thin sections were prepared from two samples (JAM-13-1b, c) for petrographic study, SEM imaging and chemical analyses of minerals by EDS (see below). Two larger samples (~0.3 kg, JAM-13-1c, e) were submitted for whole-rock chemical analyses and $^{40}\text{Ar}/^{39}\text{Ar}$ analyses.

3.2. Whole-rock chemical analyses.

The two samples (JAM-13-1c, e) selected for whole-rock geochemical analysis were crushed in a porcelain jaw crusher and powdered in a tungsten carbide shatterbox. A full suite of major- and trace-element analyses (**Table 1**) was completed at Acme Analytical Laboratories Ltd. in Vancouver, British Columbia. Major elements were measured using ICP-emission spectrometry and trace elements were measured using ICP-mass spectrometry. Both methods were completed on fused rock powders. Replicates and an internal standard were analyzed using the same procedures to

monitor the analytical reproducibility during analysis of all elements. Discrepancies among replicate analyses are <5% for the major elements, <5% for trace elements with abundances >10 ppm, and <10% for trace elements with abundances of <10 ppm.

TABLE 1. Whole-rock chemical analyses, Green Bay

Sample	JAM-13-1c	JAM-13-1e
Major elements, wt.%		
SiO ₂	51.93	50.28
TiO ₂	0.89	0.99
Al ₂ O ₃	17.30	15.67
Fe ₂ O ₃ (t)	9.71	10.96
Cr ₂ O ₃	0.01	0.02
MnO	0.19	0.20
MgO	5.01	6.44
CaO	7.62	8.83
Na ₂ O	3.38	3.12
K ₂ O	1.93	1.32
P ₂ O ₅	0.22	0.21
LOI	1.50	1.70
Total	99.69	99.74
Trace elements, ppm		
Sc	26.00	36.00
Ni	23.00	35.00
V	254.00	305.00
Co	27.00	34.10
Rb	44.50	27.00
Sr	392.10	404.50
Y	19.10	19.40
Zr	68.70	67.50
Nb	2.30	2.20
Ba	918.00	501.00
La	8.20	8.00
Ce	18.00	17.60
Pr	2.73	2.82
Nd	13.20	13.50
Sm	3.17	3.45
Eu	1.05	1.21
Gd	3.83	3.95
Tb	0.60	0.63
Dy	3.58	3.58
Ho	0.70	0.73
Er	2.02	2.13
Tm	0.30	0.30
Yb	1.82	1.85
Lu	0.28	0.27
Hf	2.10	2.00
Ta	0.20	0.20
Th	1.50	1.60
LOI—loss on ignition.		
(t)—Total iron is expressed as Fe ₂ O ₃ .		

3.3. Energy Dispersive Spectroscopy (EDS).

Chemical analyses of minerals were performed at the College of Arts and Sciences Microscope Facility, Appalachian State University. The instrument is an FEI Quanta 200 scanning electron microscope, fitted with an EDS microanalyzer (EDAX). Mineral standards were obtained from the Smithsonian Institute (USNM series). Instrument settings were 35 kV acceleration voltage, 4 μm spot size, and 50 s counting time. Raw data were processed with Genesis 3.5 software. The Genesis software has certain peculiarities regarding constraints on the ZAF algorithm. The software does not allow for using more than one standard at a time, and the sum of the weight percents of oxide components is constrained to a user-specified value. For the purpose of major-oxide analyses, except K_2O , these peculiarities were accommodated satisfactorily by choice of a suitable standard, and by paying special attention to stoichiometry (especially, atomic proportions of cations). For the silicate minerals, USNM omphacite standard (#1106067) was used. For each mineral, the sum of the weight percents of the oxide components was normalized to 100. The low K_2O in the omphacite standard (0.15 wt.%) makes it unreliable for K_2O in silicate minerals with appreciable K_2O (>1 wt.%). In order to accommodate the problem, in each EDS session the USNM microcline standard (#1143966, 15.14 wt.% K_2O) was analyzed as an unknown at the beginning of the session (5 or 6 spots) and at the end of the session (5 or 6 spots). New correction factors were calculated for the major oxides in the microcline standard (Na_2O , K_2O , Al_2O_3 , SiO_2). The new correction factors were then applied, in a fashion consistent with ZAF procedures, to mineral analyses referred to the omphacite standard (USNM #1106067). The analyses were renormalized to 100 wt.%. These analyses were then processed by the software AX (Holland and Powell, 2000), which provides an estimate of Fe_2O_3 based on cation stoichiometry and formal number of anionic charges per formula unit (pfu). The processed analyses are presented in **Tables 2** and **3**. Systematics of the cation proportions (i.e., stoichiometry) indicate that the procedure is successful within expected limits of analytical uncertainty for EDS. For the Fe-Ti oxide minerals, one standard was used, USNM ilmenite (#96189).

3.4. $^{40}\text{Ar}/^{39}\text{Ar}$ data.

Splits of the two largest samples (JAM-13-1c, JAM-13-1e, ~0.3 kg) were disaggregated, washed, and then sieved to 149-177 μm . The samples were then rinsed in warm diluted hydrochloric acid to remove carbonate minerals and rinsed again in deionized water. This fraction of sample JAM-13-1c was loaded for $^{40}\text{Ar}/^{39}\text{Ar}$

whole-rock analysis. Reflected and transmitted light microscopy of sample JAM-13-1e indicated that it contained sufficient K-feldspar and amphibole to attempt further separation. Amphibole was prepared to an optical purity of >99.9% by prolonged ultrasonic treatment along with standard magnetic and density separation techniques. K-feldspar was less abundant and there was insufficient sample to prepare a high purity separate. XRD indicates ~50% K-feldspar, ~50% plagioclase, and negligible quartz. The remaining portion of JAM-13-1e (K-feldspar and amphibole removed) was also loaded as a pseudo whole-rock analysis. Prior to packaging, all samples were washed sequentially with acetone, alcohol, and deionized water (3x) in a Branson B220 ultrasonic bath.

The washed samples were packaged in high purity copper, sealed under vacuum ($\sim 10^{-6}$ torr) into fused silica vials, and then irradiated for 30 hours in the U.S. Geological Survey TRIGA reactor in Denver, Colorado (Dalrymple et al., 1981). Fish Canyon sanidine (FC-2), with a preferred age of 27.79 Ma relative to MMhb-1 at 519.4 ± 2.5 Ma (Alexander et al., 1978; Cebula et al., 1986), was used as the flux monitor and was interspersed at ~1 cm intervals along the vial length. Annealed K_2SO_4 and optical grade CaF_2 were included in the irradiation to monitor neutron-induced interferences from K and Ca. Following irradiation, FC-2, K_2SO_4 , and CaF_2 were fused with a Synrad CO_2 laser, and unknown samples were step-heated in a low blank furnace. After cleanup of the extracted gases all argon isotopes were analyzed on an MAP-216 noble gas mass spectrometer at the U.S. Geological Survey $^{40}\text{Ar}/^{39}\text{Ar}$ geochronology laboratory in Reston, Virginia. Additional details of the analytical methods can be found in Kunk et al. (2005).

Correction factors were determined by repeat analysis of K_2SO_4 and CaF_2 and are reported in the footnotes of the data table (Appendix 1). J-factors were determined by analysis of 6 or 7 single FC-2 sanidine crystals at each monitor position, and an uncertainty of 0.25% is applied to all J-values. The reproducibility of the standard FC-2 suggests this is a conservative estimate. The calculated J-factor varies by <1% among the unknown samples analyzed for this study. Mass spectrometer sensitivity was 1.962×10^{-13} ($\pm 2.3\%$) moles/volt and mass discrimination was 1.00676 ($\pm 0.09\%$) per amu during unknown analyses. Typical blanks were 2×10^{-15} mol for ^{40}Ar , 6×10^{-17} mol for ^{37}Ar , and $<1 \times 10^{-17}$ mol for ^{39}Ar , ^{38}Ar , and ^{36}Ar . Decay constants used were those recommended by Steiger and Jäger (1977). In the data tables and figures, errors for the ages of individual increments are reported at 1σ . Plateau ages are reported where contiguous steps agree at the 95% confidence level and contain

TABLE 2. Chemical analyses of minerals, sample^a JAM-13-1c, Green Bay, Jamaica.

No. of analyses	Hornblende ^b	Chlorite ^c	Orthoclase	Plagioclase
	5	5	9	10
	Wt.% (st. dev.)			
SiO ₂	45.54 (0.24)	28.58 (0.41)	64.06 (0.49)	58.71 (0.46)
TiO ₂	0.55 (0.12)	0.50 (0.50)	0.31 (0.07)	0.09 (0.07)
Al ₂ O ₃	10.01 (0.24)	19.31 (0.51)	18.51 (0.62)	26.44 (0.31)
^d Fe ₂ O ₃	3.98 (0.09)	7.03 (0.19)	0.40 (0.09)	0.52 (0.07)
FeO	14.30 (0.31)	25.30 (0.70)	0.00	0.00
MnO	0.21 (0.05)	0.27 (0.04)	0.05 (0.03)	0.06 (0.02)
MgO	11.19 (0.23)	18.40 (0.65)	0.05 (0.01)	0.02 (0.02)
CaO	12.36 (0.22)	0.68 (0.44)	0.49 (0.19)	7.20 (0.23)
Na ₂ O	1.32 (0.12)	0.38 (0.26)	0.92 (0.20)	6.71 (0.43)
K ₂ O	0.95 (0.07)	0.25 (0.08)	15.27 (0.52)	0.30 (0.13)
Total	100.01	100.69	100.08	100.05
Oxygens pfu ^e	23	14	8	8
	Cations pfu ^e			
Si	6.63	2.67	2.96	2.62
Ti	0.06	0.04	0.01	0.00
Al	1.72	2.12	1.01	1.39
Fe ³⁺	0.44	0.49	0.01	0.02
Fe ²⁺	1.74	1.97	0.00	0.00
Mn	0.03	0.02	0.00	0.00
Mg	2.43	2.56	0.00	0.00
Ca	1.93	0.07	0.02	0.34
Na	0.37	0.07	0.08	0.58
K	0.18	0.03	0.90	0.02
Sum	15.66	10.04	5.01	4.97
Mg/(Mg+Fe ²⁺)	0.58	0.56	<i>or</i> 0.89	0.02
			<i>ab</i> 0.08	0.62
			<i>an</i> 0.02	0.37

^aMineral assemblage:

hornblende, chlorite, orthoclase, plagioclase, quartz, calcite, magnetite, ilmenite, titanite, apatite, hematite.

^bBorderline pargasite-magnesiohornblende, IMA Subcommittee on Amphibole Classification (Hawthorne et al., 2012).^cSheridanite, close to clinocllore.^dFe₂O₃ estimated by computer program AX.^epfu=per formula unit. Formula calculated by computer program AX.

>50% of the ³⁹Ar_K. In sample JAM-13-1e where the apparent ages of consecutive steps are similar, but do not satisfy the formal criteria for a plateau age, the weighted average age for the consecutive steps is reported. MassSpec V 7.79 (Deino, 2014) was used for machine automation and all data analysis. Complete isotopic data are reported in the [Appendix 1](#).

3.5. Thermodynamic calculations

Activities of mineral components were calculated using the software AX (Holland and Powell, 2000). Thermodynamic calculations were performed using the software THERMOCALC, v. tc325, data set 5.5, 12 November 2004 (Holland and Powell, 1998; Powell et al., 1998; Powell, 2005). Henceforth, these programs are simply cited as AX and THERMOCALC.

4. PETROGRAPHY AND MINERAL CHEMISTRY

The Green Bay Inlier consists mainly of fine-grained (~0.25 mm), well-foliated hornblende schist (**Figure 3A, B**). The mineral assemblage consists of hornblende (~35%), plagioclase (~45%), orthoclase (~10%), chlorite (~5%), and quartz (~5%), and trace amounts of calcite, titanite, magnetite, ilmenite, and apatite. Locally, the rock has narrow (~5 mm), diffuse, or otherwise weakly developed, mafic laminae, for the most part apparent only on weathered surfaces (**Figure 3A**). The mafic laminae are distinguished from the rest of the rock by a higher proportion of hornblende. Otherwise the mineral assemblage is the same throughout.

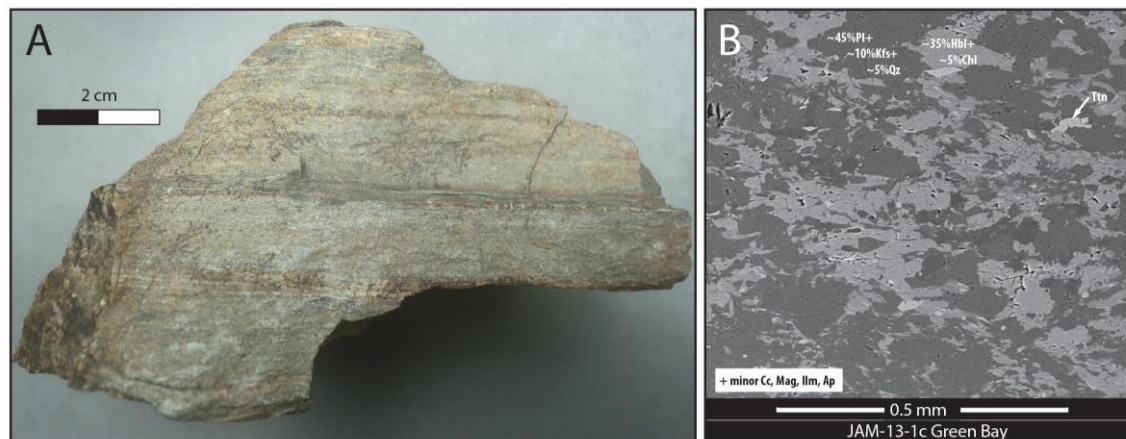


Figure 3. A. Weathered surface of hand specimen. The banding reflects variations in hornblende content (dark, more hornblende; light, less hornblende). Fresh surfaces are uniformly black and otherwise uninspiring. B. SEM image of a polished thin section of Green Bay Schist, sample JAM-13-1c. Plagioclase, K-feldspar and quartz are dark gray. Quartz is a slightly darker shade of gray than plagioclase and K-feldspar. Hornblende and chlorite are light gray. The brightest grains are titanite. The mean grain size is ~0.25 mm.

4.1. Silicate minerals.

Average compositions of hornblende, chlorite, orthoclase and plagioclase are reported in **Table 2**. There is nothing particularly unusual about the compositions of these minerals. In the formal nomenclature for amphiboles (**Hawthorne et al., 2012**), the hornblende is borderline pargasite-magnesianhornblende. The chlorite is of the variety sheridonite, close to clinochlore (Wiewiora and Weiss, 1990). The $Mg\# = 100 * Mg / (Fe + Mg)$ is nearly the same in both minerals, 58 in the hornblende and 56 in the chlorite. The plagioclase is andesine (ab_{62}); the orthoclase is appreciably sodic (ab_{08}). The titanite is near stoichiometric $CaTiSiO_5$.

4.2. Fe-Ti oxides.

Magnetite occurs as minute (~0.05 mm), isolated, subhedral to euhedral grains. Ilmenite occurs as even smaller (~0.02 mm), more-or-less equidimensional, anhedral grains. Ilmenite grains are clad by thin (~0.005 mm) rims of titanite. Average compositions for magnetite and ilmenite are reported in **Table 3**. The analyses are noteworthy only for the high Mn-content of the ilmenite (16% $MnTiO_3$ “pyrophanite”).

5. WHOLE-ROCK GEOCHEMISTRY

5.1. Major elements: protolith characteristics.

Normative calculations were performed using an Excel spreadsheet designed by **Hollocher (nd)**, see reference for website). The calculations assumed a value of $Fe_2O_3 / (FeO + Fe_2O_3) = 0.35$, typical for

basaltic compositions (e.g., **Best and Christiansen, 2001**). The resulting average major-element chemistries for Green Bay Schist, Westphalia Schist (**West et al., 2014**) and Mt. Hibernia Schist (**West et al., 2014**) are reported in **Table 4**, along with the normative mineralogy. With regard to the protoliths, **Hollocher’s (nd)** spreadsheet also provides various useful differentiation parameters, a selection of which is reported in **Table 4**.

Pearce (2014) offers a cautionary note regarding the use of major elements for classification of magma type (e.g., TAS, total alkali–silica) in volcanic rocks that have been metamorphosed or otherwise altered. Of course, this concern extends to normative analyses and differentiation parameters such as those reported in **Table 4**. With this in mind, the differentiation parameters would suggest that the protoliths could be ordered from the least differentiated (most primitive) Mt. Hibernia Schist, to Green Bay Schist, to the most differentiated (least primitive) Westphalia Schist. However, the high normative quartz and low normative plagioclase in Mt. Hibernia Schist sets it apart from Green Bay Schist and Westphalia Schist in a way that would be very difficult to reconcile with normal processes of fractionation during melting or crystallization. Also, the $Mg\#$ does not decrease from Mt. Hibernia Schist to Green Bay Schist, contrary to expected trends during melting or crystallization. On the basis of major elements alone, it would seem that the Mt. Hibernia “magma” is not related to the Green Bay and Westphalia “magmas.” There are no such obvious indications that Green Bay and Westphalia “magmas” are unrelated. The major elements indicate that the Westphalia “magma” could be

derived by crystal fractionation from the Green Bay “Magma,” that is to say, the latter is somewhat, but distinctly, more primitive than the former. However, the difference could be explained equally well by the amount of melting in the same source region, in which case, the Green Bay “magma” would represent a greater amount of melting than the Westphalia “magma.” Incompatible, immobile elements offer more compelling evidence.

5.2. Incompatible, immobile elements

Recently, a very clear and concise procedure for interpreting incompatible, immobile–element data became available in an article by Pearce (2014) in a special issue of *Elements* (2014, April) devoted to ophiolites. The procedure, involving various

immobile–element discrimination diagrams, is directly relatable to West et al.’s (2014) interpretation of data for Westphalia Schist and Mt. Hibernia Schist. For the immediate purpose of comparing Green Bay Schist to Westphalia Schist and Mt. Hibernia Schist, West et al.’s (2014) data are replotted and interpreted here in the framework of Pearce’s (2014) procedure.

The point of departure for Pearce’s (2014) procedure is the incompatible, immobile–element patterns portrayed in Figure 4. Analyses are normalized to N-MORB (Sun and McDonough, 1989). The elements are ordered according to increasing compatibility. For pairs of elements that behave in a similar fashion (Ta–Nb, Hf–Zr, Ho–Y), the average of the two values of the pair is used. The pattern for Mt. Hibernia Schist classifies as P-MORB (Plume) (Pearce, 2014). This is consistent

TABLE 3. Chemical analyses of oxides, sample^a JAM-13-1c, Green Bay, Jamaica.

No. of analyses	Ilmenite	Magnetite
	5	8
	Wt.% (st.dev.)	
TiO ₂	52.49 (0.83)	0.38 (0.14)
^b Fe ₂ O ₃	0.51 (0.01)	68.37 (0.27)
FeO	39.69 (5.09)	30.35 (0.13)
MnO	7.31 (4.73)	0.70 (0.28)
MgO	0.06 (0.06)	0.21 (0.14)
Total	100.06	100.01
Oxygens pfu ^c	3	4
	Cations pfu ^c	
Ti	1.00	0.01
Fe ³⁺	0.01	1.98
Fe ²⁺	0.84	0.98
Mn	0.16	0.02
Mg	0.00	0.01
Sum	2	3
<i>ilm</i> ^d	0.84	
<i>hem</i>	0.01	
<i>pph</i>	0.16	
	<i>mag</i> ^d	0.96
	<i>usp</i>	0.01
	<i>mfr</i>	0.01
	<i>jac</i>	0.02

^aMineral assemblages:

hornblende, chlorite, orthoclase, plagioclase, quartz, calcite, magnetite, ilmenite, titanite, apatite, hematite.

^bFe₂O₃ estimated by computer program AX.

^cpfu=per formula unit. Formula calculated by computer program AX.

^dabbreviations:

ilm (ilmenite) = FeTiO₃
hem (hematite) = Fe₂O₃
pph (pyrophanite) = MnTiO₃
mag (magnetite) = Fe₃O₄
usp (ulvospinel) = Fe₂TiO₄
mfr (magnesianoferrite) = MgFe₂O₄
jac (jacobsite) = MnFe₂O₄

TABLE 4. Whole-rock, major-element chemistry^a

Sample no. analyses	Ave. GBS ^b 2	Ave. WS 9	Ave. MHS 8
Major elements (wt.%), assuming Fe ₂ O ₃ /(FeO+Fe ₂ O ₃) = 0.35 (wt.)			
SiO ₂	52.50	55.55	51.35
TiO ₂	0.97	0.78	0.72
Al ₂ O ₃	16.94	16.65	15.39
Fe ₂ O ₃	3.68	2.53	4.48
FeO	6.14	4.23	7.49
MnO	0.21	0.20	0.18
MgO	5.89	2.83	7.16
CaO	8.45	10.39	10.81
Na ₂ O	3.34	3.57	2.19
K ₂ O	1.67	3.00	0.13
P ₂ O ₅	0.23	0.28	0.09
Total	100.02	100.01	99.99
Normative wt. %			
Quartz	0.29	1.74	4.93
Plagioclase	54.56	50.75	50.31
Orthoclase	9.87	17.73	0.77
Diopside	11.04	23.83	17.23
Hypersthene	16.17	0.16	18.68
Ilmenite	1.84	1.48	1.37
Magnetite	5.34	3.67	6.50
Apatite	0.51	0.65	0.21
Other parameters			
100*Mg/(Mg+Fe _{total})	52.63	43.67	52.56
An ^{pl}	46.72	39.06	61.78
Differentiation index	64.72	70.22	56.01
Estimated liquidus T (°C)	1168	1112	1189

^aRecalculated using Excel spreadsheet from Hollocher, K. (nd).

Norm 4: norm calculation program.

web site: minerva.union.edu/hollochkc/petrology/norms.htm

^bGBS=Green Bay Schist, WS=Westphalia Schist, MHS=Mt. Hibernia Schist

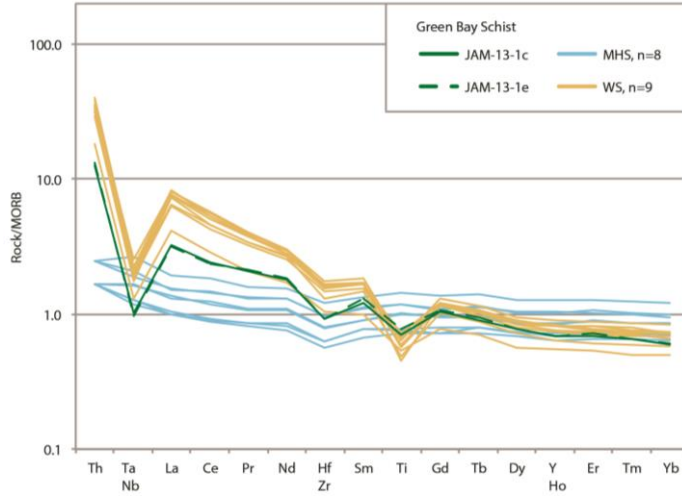


Figure 4. Incompatible, immobile N-MORB-normalized patterns (after [Pearce, 2014](#)) for Westphalia Schist, Mt. Hibernia Schist and Green Bay Schist. The data for Westphalia Schist and Mt. Hibernia Schist are from [West et al. \(2014\)](#). The patterns for Green Bay Schist and Westphalia Schist are very similar, both consistent with C-MORB classification (contaminated), according to [Pearce \(2014\)](#). That the patterns for Green Bay Schist are of lower slope than most of the patterns for Westphalia Schist suggest that Green Bay magma was slightly more primitive (or less differentiated) than the Westphalia magma, but related paragenetically. The pattern for Mt. Hibernia Schist is consistent with P-MORB (plume) according to [Pearce \(2014\)](#).

with the interpretation of [West et al. \(2014\)](#); and see [Hastie et al., 2008](#)). Green Bay Schist and Westphalia Schist both classify as C-MORB (contaminated), very close to the “Taitao, Chile” example of a subducted ridge ([Pearce, 2014](#)). The similarity in the patterns for Green Bay Schist and Westphalia Schist serves as the most compelling evidence that the protoliths for Green Bay Schist and Westphalia Schist are very closely related, if not equivalent. The subtle difference in slope can be explained by the either fractional crystallization or fractional melting; in either case, consistent with the behavior of the major elements.

5.2.1 Proxy for TAS rock classification

For metamorphosed rocks, where major elements may have been affected, the Zr/Ti–Nb/Y diagram ([Figure 5](#)) is a well-tested proxy for the standard TAS (total alkali–silica) diagram ([Pearce, 2014](#)). While protoliths for Mt. Hibernia Schist and Green Bay Schist both classify as basalt, and plot close

together, other attributes indicate that the two are distinct with regard to magma type, i.e., major elements ([Table 4](#)) and incompatible, immobile-elements patterns ([Figure 4](#)). The protolith for Westphalia Schist classifies as basaltic andesite. Again, the difference between Westphalia Schist and Green Bay Schist can be explained by either fractional crystallization or fractional melting.

5.2.2 Magma type and tectonic setting

The Th/Yb–Nb/Yb diagram ([Figure 6](#)) effectively distinguishes between MORB–OIB (OIB=oceanic island basalt) environments and oceanic arc environments ([Pearce, 2014](#)). Analyses for Mt. Hibernia Schist plot in the MORB-OIB array, between N-MORB and E-MORB, consistent with [Pearce’s \(2014\)](#) “Nicoya” example of P-MORB. Analyses of Mt. Hibernia Schist plot among the subduction-unrelated plume-type basalts of [Dilek and Furnes \(2014\)](#). Both Green Bay Schist and Westphalia Schist plot in the calc-alkaline part of

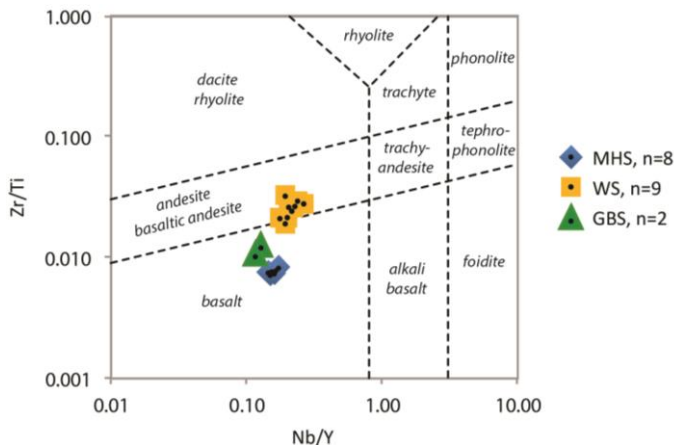


Figure 5. Zr/Ti–Nb/Y proxy for TAS (total alkali, silica) classification volcanic rocks ([Pearce, 2014](#)). Green Bay Schist (this study) and Mt. Hibernia Schist ([West et al., 2014](#)) plot close together in the basalt field. Most of the analyses for Westphalia Schist ([West et al., 2014](#)) plot in the andesite/basaltic andesite field. Again, the difference between Green Bay Schist and Westphalia Schist is consistent with the magma for the former being more primitive (or less differentiated) than the magma for the latter.

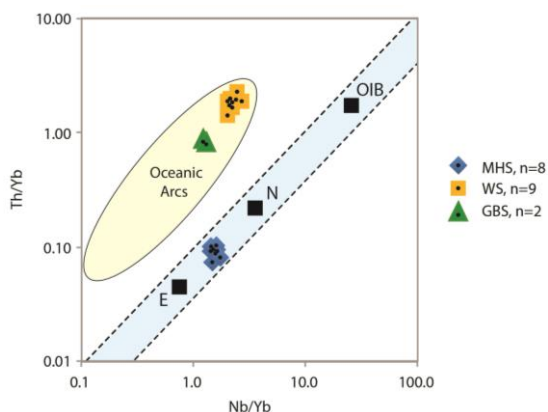


Figure 6. Th/Yb–Nb/Yb discriminant diagram (Pearce, 2014) for distinguishing between suprasubduction zone (SSZ) and MORB-OIB tectonic environments. Data for Green Bay Schist and Westphalia Schist plot in the Oceanic Arc field, in a way that is consistent with the magma for the former being more primitive (or less differentiated) than the magma for the latter. Mt. Hibernia Schist plots in the MORB-OIB field.

the oceanic arc region (Pearce, 2014). According to Dilek and Furnes (2014), Green Bay Schist and Westphalia Schist would be classified as subduction-related, calc-alkaline basalt.

5.2.3 Subdivisions of tectonic setting

Figure 7 portrays subdivisions of the MORB-OIB array and subdivisions of supra-subduction zone (SSZ) basalt (Pearce, 2014). The bold, sub-horizontal, dashed lines in Figure 7A define two regions, distinguished by the depth of melt production. MORB is related to shallow melting; OIB is related to deep melting. The shaded region corresponds to plume-ridge interaction at various depths. Analyses of Hibernia Schist plot in the shallow-melting region, related to mantle plume, i.e., P-MORB. The V-Ti plot in Figure 7B gives information regarding the influence of H₂O, a signature for melting above the subduction zone or contamination of magma ascending through the SSZ. The island arc tholeiite (IAT) and boninite fields indicate melting above the subduction zone. The MORB field indicates melt production beneath the subduction zone (Pearce, 2014; Dilek and Furnes, 2014). Green Bay Schist and Westphalia Schist both plot in the MORB region, variously affected in the SSZ region, i.e., C-MORB. V-Ti values close to the boundary with the IAT indicate a greater amount of contamination in the SSZ.

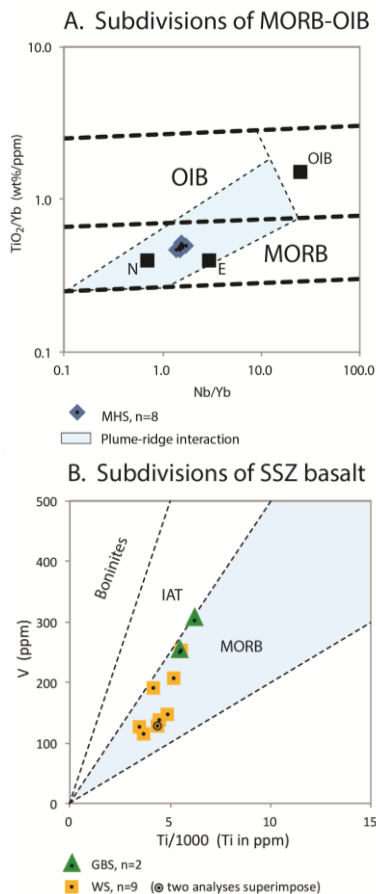


Figure 7. A. Subdivisions of MORB-OIB (Pearce, 2014). Mt. Hibernia Schist plots in the shaded field for interaction between plume and ridge. B. Subdivision of supra-subduction zone (SSZ) basalt (Pearce, 2014). Green Bay Schist and Westphalia Schist both plot in a field for SSZ MORB, i.e., a mantle source below a subduction zone.

6. ⁴⁰Ar/³⁹Ar GEOCHRONOLOGY

Analytical results from ⁴⁰Ar/³⁹Ar step-heating experiments are presented in the Appendix 1. ³⁹Ar release spectra are shown in Figure 8. Amphibole (Figure 8A) and K-feldspar (Figure 8B) (Section 6.1) both have reasonably well constrained closure temperatures (discussed below), and thus provide points on a cooling history (T-t). Whole-rock data (Figure 8C, D) (Section 6.2) provide ages that are not readily temperature-constrained, but are nevertheless related to cooling.

6.1. JAM-13-1e amphibole and K-feldspar results

The amphibole age spectrum for sample JAM-13-1e (Figure 8A) is only moderately discordant, with most of the discordance in the lower radiogenic yield, initial and final heating steps, possibly

reflecting minor impurities of, or alteration to, chlorite and titanite (**Figure 3**). The apparent ages are in a narrow range from 55.9 to 61.1 Ma for 8 of the 12 heating steps (98.4% of the $^{39}\text{Ar}_K$). Apparent K/Ca ratios vary little throughout the heating steps, suggesting a relatively uniform amphibole composition as expected, based on the optical purity of the concentrate. A weighted average age of 60.7 ± 0.8 Ma is calculated for 76.5% of the total ^{39}Ar released. This age is interpreted to reflect the time of cooling below $\sim 500^\circ\text{C}$ (**McDougall and Harrison, 1999**) following amphibolite facies metamorphism.

The age spectrum from the K-feldspar concentrate from sample JAM-13-1e (**Figure 8B**) also exhibits minor discordance, with apparent ages ranging from 58.0 to 62.3 Ma for 15 of the 18 heating steps (98.5% of the $^{39}\text{Ar}_K$). A “mini” plateau age of 58.3 ± 0.2 Ma is calculated for 8 heating steps that contain 48.7% of the $^{39}\text{Ar}_K$. The high radiogenic yields (>90%) of each of these steps is consistent with the degassing of primarily K-feldspar, while the K/Ca values are ~ 10 , suggesting minor contribution of Ca-derived ^{37}Ar from plagioclase. Higher apparent ages and lower radiogenic yields during the heating steps associated with the latter half of the experiment suggest greater contributions from plagioclase.

The assignment of a unique closure temperature to K-feldspar is difficult under the best of circumstances (see recent reviews in **Harrison and Lovera, 2013**; **Villa, 2013**) and would be particularly tenuous in the present case, given the impure nature of the K-feldspar concentrate. However, given the minor age variation across the entire age spectrum and the agreement of steps with the highest radiogenic yield, we interpret the 58.3 ± 0.2 Ma mini-plateau age to approximate a time of rapid post-peak metamorphic cooling from ~ 250 to $\sim 150^\circ\text{C}$ (**Harrison and McDougall, 1982**).

6.2. Whole-rock results

The spectra from the remaining components of sample JAM-13-1e (labeled “whole-rock” in **Figure 8C**) and the whole-rock analysis of JAM-13-1c, collected only meters away, are both relatively uncomplicated. The samples record overlapping integrated ages of 57.8 and 57.6 Ma, respectively. Four steps in sample JAM-13-1c meet the statistical criteria for a plateau age of 57.69 ± 0.17 Ma (61.7% of the $^{39}\text{Ar}_K$). The samples also degas similarly in-vacuo as indicated by similar K/Ca, $^{40}\text{Ar}^*$, and age patterns during the step-heating experiments (**Appendix 1**). We

suggest that the samples record the same post-metamorphic cooling history. Unfortunately, a specific closure temperature cannot be assigned to whole-rock ages from metamorphic rocks (**McDougall and Harrison, 1999**). Instead, the whole-rock ages reflect the combined effects of variable cooling ages of the K-bearing minerals, excess argon, and alteration. Nevertheless, it should be noted that our best estimate for the timing of cooling below K-feldspar closure-temperatures ($150\text{--}250^\circ\text{C}$, 58.3 ± 0.2 Ma) and the whole-rock ages (56 to 58 Ma) are similar, and both are only slightly younger than the timing of cooling below the amphibole closure-temperature (500°C , 60.7 ± 0.8 Ma). Therefore, while the specifics of closure temperatures can be debated, it is abundantly clear that Green Bay Schist cooled very quickly in the interval between about 60 and 56 Ma, and has remained relatively cold ($<250^\circ\text{C}$) since that time.

7. THERMODYNAMIC CALCULATIONS

Figure 9 portrays the results of thermodynamic calculations involving components in hornblende, chlorite, plagioclase and orthoclase (**Table 2**), coexisting with quartz, calcite and an $\text{H}_2\text{O}\text{--}\text{CO}_2$ fluid. Equilibrium between plagioclase and K-feldspar provides the strongest constraint on the temperature (**Section 7.1**). Equilibrium *r5* (**Table 5**) provides the strongest constraint on the pressure (**Section 7.2**). The “average T” option in THERMOCALC (reactions *r1*, *r2*, *r3*, *r4*, **Table 5**) provides an estimate of the CO_2 content of an aqueous fluid (**Section 7.2**). Finally, magnetite-ilmenite equilibrium provides an independent estimate of the temperature and $f(\text{O}_2)$ (**Section 7.3**).

7.1. Feldspar equilibrium

In addition to estimating Fe_2O_3 and providing a chemical formula (cations pfu) from chemical analyses (**Table 2, 3**), the software AX also calculates the activities of mineral components. For coexisting feldspars, it is a simple matter to perform a search for the equilibrium conditions (P, T) where the activities of the feldspar components are the same in both feldspars. Because of low Ca in the orthoclase and low K in the plagioclase, this approach is only practical for the Na component, $X_{\text{ab}}^{\text{Kfs}} = 0.08$, $X_{\text{ab}}^{\text{Pl}} = 0.62$ (**Table 2**). The result of this simple exercise gives 510°C , regardless of the pressure. The pressure-dependent formulation developed by **Stormer (1975)** for two-feldspar thermometry gives comparable results, notably in the range from 501°C (7 kbars) to 522°C (9 kbars).

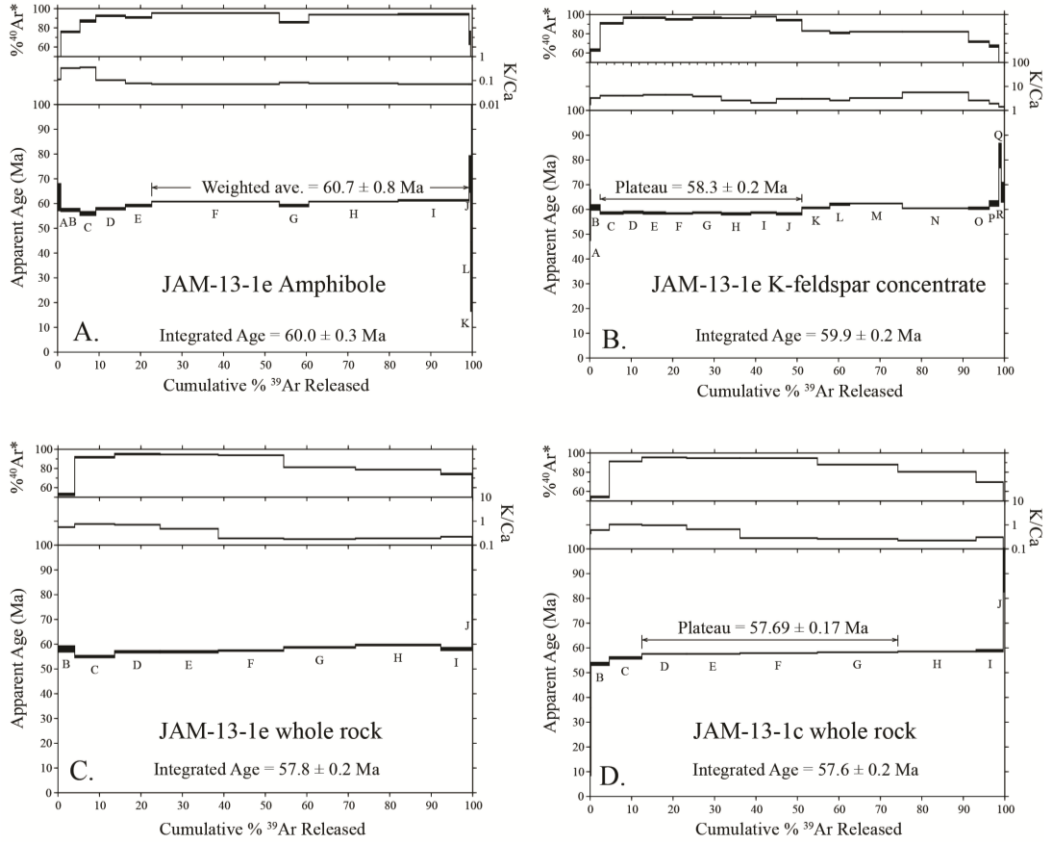


Figure 8. $^{40}\text{Ar}/^{39}\text{Ar}$ age spectra for Green Bay Schist. Analytical data are in the Appendix 1. A. Amphibole concentrate (JAM-13-1E). B. K-feldspar concentrate (JAM-13-1E). C. Whole-rock (JAM-13-1E). D. Whole-rock (JAM-13-1C).

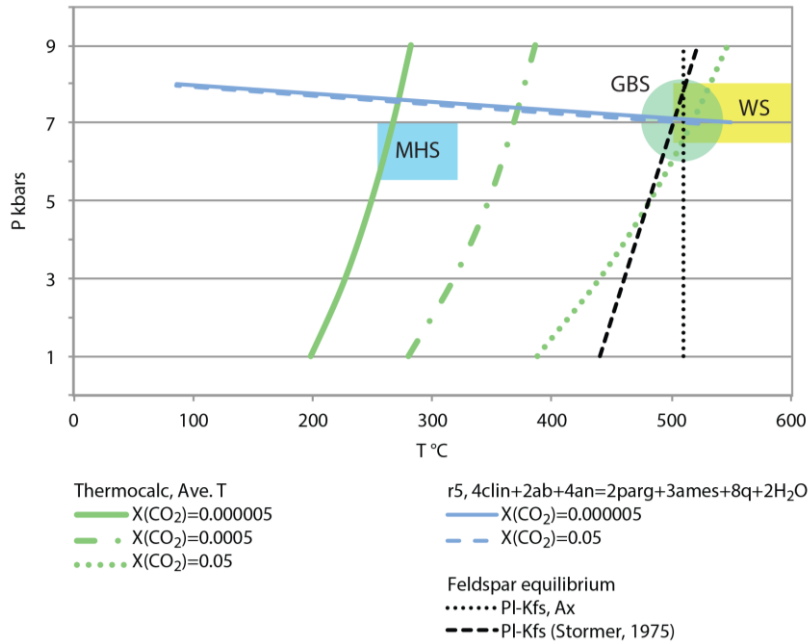
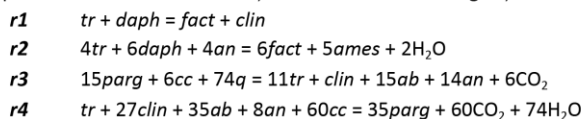
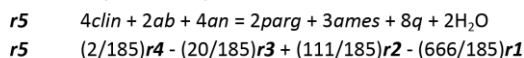
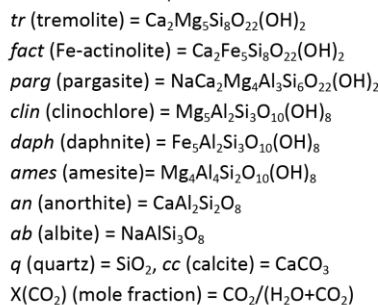


Figure 9. Equilibria described in the text and in Table 5. Equilibrium conditions (green circle) for the Green Bay Schist are $P \sim 7$ kbars, $T \sim 500^\circ\text{C}$, $X(\text{CO}_2) \sim 0.05$. The radius of the circle describes approximately the uncertainty in T ($\pm 37^\circ\text{C}$) and P (± 1.1 kbars), based on equilibrium r5 (Table 5). Blue rectangle = estimated P-T conditions for peak metamorphism in blueschist of the Mt. Hibernia Schist (Willner et al., 1995). Yellow rectangle = calculated retrograde P-T conditions for Westphalia Schist (Abbott et al., 1996; Abbott and Bandy, 2008).

TABLE 5. Reactions used in THERMOCALC.¹Independent set of four reactions, used to calculate average T, at various P and X(CO₂).²Reaction of very low dP/dT , used to calculate P at various T and X(CO₂), in the range 50-550°C.¹Abbreviations for mineral components are those used by THERMOCALC.²T=50-550°C, st. dev.(T)=37°C; st. dev.(P)=1.1 kbars $dP/dT = -0.0012$ kbars/°C at X(CO₂)=0.000005 $dP/dT = -0.0032$ kbars/°C at X(CO₂)=0.05

7.2. THERMOCALC

Calculations using the “average T” option in THERMOCALC involved an independent set of four equilibria (**r1**, **r2**, **r3** and **r4** in **Table 5**). The results depend strongly on the composition of the fluid, expressed as $X(CO_2) = CO_2/(H_2O + CO_2)$, and are consistent with the an overall reaction of the form, $A = B + CO_2 + H_2O$. Results (**Figure 9**) were calculated at various values for $X(CO_2) = 0.000005, 0.0005, \text{ and } 0.05$.

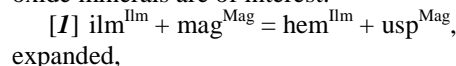
During the course of the calculations, using a THERMOCALC option that determines all possible equilibria within a specified range of P and T for a given X(CO₂), equilibrium **r5** was identified as having an unusually low, negative dP/dT slope in the range range 50-550°C, and being nearly independent of X(CO₂). The reaction is an otherwise obscure linear combination of **r1**, **r2**, **r3** and **r4** (**Table 5**). Regardless of X(CO₂) for temperatures at least up to 550°C, the calculated pressure is in the narrow range 7-8 kbars. The reaction involves no Fe-components, hence is not subject to vagaries in the estimation of Fe³⁺ in the hornblende and chlorite.

Regardless of X(CO₂), solutions to equilibrium **r5** intersect the two-feldspar equilibria at approximately 7 kbars and 500°C. The “average T” calculations indicate that the solution for X(CO₂) = 0.05 agrees most closely with these conditions. Excluding for the moment the Fe-Ti oxide minerals, these are the conditions under which the

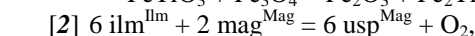
mineral assemblage would be in equilibrium. That the chlorite is late and appears undeformed indicates that the conditions, like those for Westphalia Schist, mark closure for mineral reactions on a retrograde path, i.e., cooling and decompression. The calculated P-T conditions for Green Bay Schist just happen to be similar to the P-T conditions calculated for Westphalia Schist (529-587°C, 6.2-8.6 kbars, **Abbott and Bandy, 2008**). However, a note of caution is in order. Thermochronological data (this study; **West et al., 2014**) indicate that the calculated P-T conditions for Westphalia Schist pertain to the Late Cretaceous, whereas the calculated P-T conditions for Green Bay Schist pertain to the early Paleocene.

7.3. Fe-Ti oxides.

Two equilibria involving components of Fe-Ti oxide minerals are of interest:



expanded,



expanded,



The two equilibria [1, 2] are the basis for several formulations of a widely used thermo-oxybarometer, e.g., **Spencer and Lindsey (1981)**, **Ghiorso and Sack (1991)**, and **Sauerzapf et al. (2008)**. Unfortunately, the composition of the

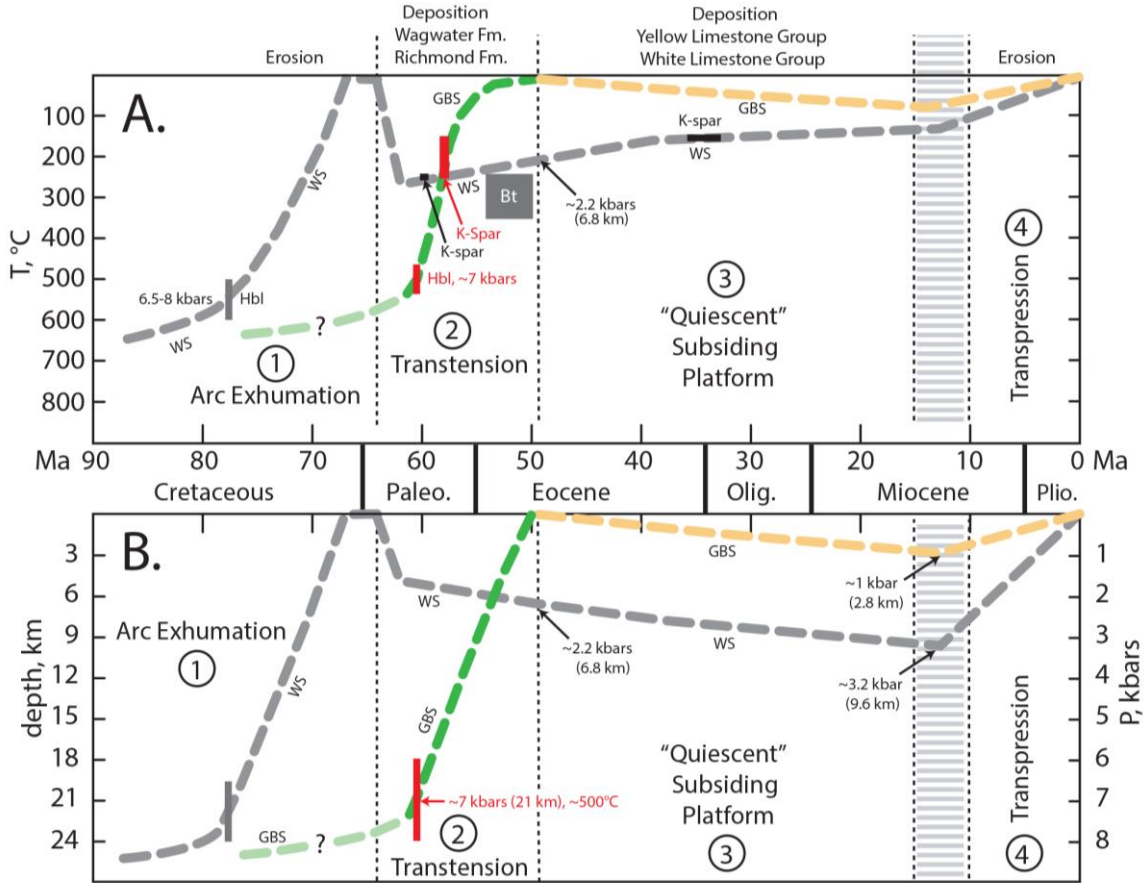


Figure 10. T-time (A) and P-time (B) paths for Green Bay Schist (GBS) and Westphalia Schist (WS). A. The thermal history for Westphalia Schist (gray) is from West et al. (2014). The thermal history for Green Bay Schist (this study) is shown in green in tectonic stages 1 and 2 (lighter green where poorly constrained), and in yellow for tectonic stages 3 and 4. Black rectangles “K-spar” = $^{40}\text{Ar}/^{39}\text{Ar}$ ages for K-feldspar in Westphalia Schist (West et al., 2014). Gray rectangles = K-Ar ages for Westphalia Schist (Lewis et al., 1973), Hbl = hornblende, Bt = biotite. Red bars = $^{40}\text{Ar}/^{39}\text{Ar}$ ages for Green Bay Schist (this study), Hbl = hornblende, K-spar = K-feldspar. The length of each red bar expresses the range of Ar-blocking temperature. B. Inferred P-time paths for Westphalia Schist (West et al., 2014) and Green Bay Schist (this study). The length of the red bar expresses the uncertainty in the calculated pressure (± 1.1 kbars, Table 5 footnote).

titanomagnetite in this study (Table 3) is outside the limits of applicability for these formulations, specifically with regard to the very low ulvospinel-content ($\text{usp} = 0.01$). Nevertheless, with a conservative extrapolation the thermo-oxymeters of Saurzapf et al. (2008) and Ghiorso and Sack (1991) give comparable estimates for a temperature less than $\sim 500^\circ\text{C}$ and $f(\text{O}_2)$ greater than $\sim 10^{-18}$. This maximum temperature is consistent with the equilibrium conditions for the silicate minerals and calcite.

8. P-T-TIME PATH

Figure 10 compares the proposed P-T histories for Green Bay Schist (this study) and Westphalia Schist (West et al., 2014; Abbott et al., 2013). The

relationships are portrayed in two diagrams, T-time (A) and P-time (B). The equivalence of the protoliths for Green Bay Schist and Westphalia Schist suggests that the prograde parts of the Mesozoic P-T histories for the two were similar (Figure 10A, B) up to the middle Campanian (~ 78 Ma). After this time, the P-T histories of the two schists diverged dramatically. From the middle Campanian to the end of the Maastrichtian the P-T history (78–66 Ma) for Green Bay Schist (light green, Figure 10A, B) is largely speculative, predicated on (1) arc-related metamorphism (maximum T, ~ 80 Ma), and (2) protracted residence time at depth (~ 20 km, ~ 7 kbars). At the beginning of the Paleocene (~ 66 Ma), Westphalia Schist was exposed at the surface ($\sim 25^\circ\text{C}$) (e.g., West et al., 2014). There is no evidence that Green Bay Schist

was exposed at the surface at this time. The nonconformity at the base of the limestone at Green Bay only indicates that Green Bay Schist was exposed at the surface (25°C) in the early Eocene (~50 Ma). Westphalia Schist shows evidence of an early Paleocene heating event consistent with a peak temperature of approximately 250°C at ~60 Ma (Abbott et al., 2013; West et al., 2014). This heating event (Figure 10A) may have been related to magmatism at the beginning of transtensional stage 2 (Abbott et al., 2013; West et al., 2014). At the same time, the $^{40}\text{Ar}/^{39}\text{Ar}$ data presented here indicate that Green Bay Schist experienced temperatures in excess of ~500°C at a depth of ~20 km (~7 kbars) (Figure 10A, B). From earliest late Paleocene to early Eocene, Green Bay Schist cooled much faster from a higher temperature (~500°C to ~25°C, 60-50 Ma) than Westphalia Schist (~250°C to ~200°C, 60-50 Ma, Abbott et al., 2013; West et al., 2014) (Figure 10A). In this same interval, Green Bay Schist was being uplifted simultaneously with the burial of Westphalia Schist beneath Wagwater and Richmond Formations (Figure 10B).

The thickness of middle Eocene to Miocene limestone varies from ~0.9 km (Draper, 2008) to ~2.8 km (Mann and Burke, 1990), which translates to a maximum pressure of ~0.9 kbars (3 km ~1 kbar) at the base of the limestone by the end of tectonic stage 3 (Figure 10B). Assuming an average geothermal gradient of ~100°C/kbar (Spear, 1993), the temperature at the base of the limestone at Green Bay (Figure 10A) would not have exceeded ~100°C at 10-15 Ma (Abbott et al., 2013), when limestone deposition ceased and tectonic stage 4 transpression commenced (Draper, 2008).

9. DISCUSSION AND CONCLUSIONS

Immobile, incompatible trace-element patterns for Westphalia Schist (West et al., 2014) and Green Bay Schist (this study) are remarkably similar. Collectively, the data strongly suggest that Westphalia Schist and Green Bay Schist are equivalent with respect to protolith composition, confirming previous speculation (e.g., Kemp, 1971; Draper, 1979, 1987). The small discrepancies in the trace-element patterns are consistent with varying degrees of either fractional melting in the magma source region or varying degrees of fractional crystallization during magma ascent. The tectonic environment for both involved subduction of an ocean ridge. The original magmas both classify as C-MORB. Immobile, incompatible trace-element patterns for Mt. Hibernia Schist bear

no resemblance to those for Green Bay Schist and Westphalia Schist. The trace-element data for Mt. Hibernia Schist indicate a mantle-plume source. The original magma classifies as P-MORB (West et al., 2014).

Calculated P-T conditions for Green Bay Schist (~500°C, ~7 kbars) are related to cooling and decompression. The conditions are very similar to retrograde conditions calculated for Westphalia Schist (Abbott and Bandy, 2008), but the timing is different (Figure 10A, B). Retrograde conditions for Westphalia Schist occurred during the Late Cretaceous, while the retrograde conditions for Green Bay Schist occurred in the Paleocene/early Eocene. Whereas Westphalia Schist was demonstrably exposed at the surface by ~66 Ma, Green Bay Schist was not exposed at the surface until ~50 Ma.

The Wagwater and Richmond Formations are missing at Green Bay, hence there is no depositional record of stage 2 transtensional tectonics. East of the Wagwater Fault, the minimum combined thickness of the Wagwater and Richmond Formations indicates a minimum displacement of 6.8 km (Mann and Burke, 1990) on the fault in transtensional stage 2. However, the metamorphic pressure calculated here for the Green Bay Schist (~7 kbars) shows that the displacement on the Wagwater Fault in transtensional stage 2 may have been very much greater, at least ~20 km. Of course, uplift of the Green Bay Schist in transtensional stage 2 was not necessarily accommodated solely by displacement on the Wagwater Fault. Some of the uplift may have been accommodated by structures yet to be discovered between Green Bay and the Wagwater Fault. Nevertheless, we conclude that the depth-time relationships in transtensional stage 2 (65-50 Ma, Figure 10B) are consistent with normal motion on the Wagwater Fault, inasmuch as the footwall (Green Bay Schist) moved up while the hanging wall (Westphalia Schist) moved down.

Deposition of the Yellow and White Limestone Groups in tectonic stage 3 (50-10 Ma, Figure 10B) took place both to the east and west of the Wagwater Fault. The combined thickness of the limestone groups approaches ~2.8 km, (Mann and Burke, 1990). It follows that in transpressional stage 4, starting ~10 Ma, as much as 2.8 km of uplift (~0.3 mm/y) has occurred at Green Bay. East of the Wagwater Fault, the combined thickness of the stage 2 redbeds (Wagwater and Richmond Formations) and the stage 3 limestone (Yellow and White Limestone Groups) indicates at least 9.6 km of uplift (>1 mm/y) in transpressional stage 4 (Abbott et al., 2013; West et al., 2014). We conclude that the stratigraphic control in

transpressional stage 4 (10-0 Ma, **Figure 10B**) is consistent with reactivation of the Wagwater Fault with reverse motion, inasmuch as the upward displacement of the footwall (Green Bay Schist) is less than the upward displacement of the hanging wall (Westphalia Schist). This is consistent with the current paradigm regarding recent and ongoing tectonic activity (e.g., **Mann et al., 1985; Robinson, 1994; Draper, 2008; Dominguez-Gonzalez et al., 2015**).

Acknowledgements. We are indebted to Colonel Desmond Edwards and Major Richard A. DaCosta of the Jamaican Defense Force for making possible our visit to Green Bay. We appreciate the time and patience of Dr. Guichuan Hou, director of the College of Arts and Sciences Microscope Facility, Appalachian State University. We are grateful for the helpful comments of USGS reviewers Dr. Arthur Merschat and Dr. Bruce Taggart, CJES reviewers, and editor Dr. Sherene James-Williamson. We thank Prof. Simon F. Mitchell for his ever helpful consultation. Any use of trade, firm, or product names is for descriptive purposes only and does not imply endorsement by the U.S. Government.

REFERENCES

- Abbott, R. N., Jr. and Bandy, B. R. 2008.** Amphibolite and Blueschist-Greenschist Facies Metamorphism, Blue Mountain Inlier, Eastern Jamaica. In: **S. K. Donovan (Ed.)**, *Geological Crustal and Biotic Evolution of the Caribbean Plate: A tribute to T.A. Jackson*. *Geological Journal*, **43**, 525-541, DOI: 10.1002/gj.1126.
- Abbott, R. N., Jr., Bandy, B. R., Jackson, T. A. and Scott, P. W. 2003.** Blueschist-greenschist transition in the Mt. Hibernia Schist, Union Hill, Jamaica. *International Geology Review*, **45**, 1-15.
- Abbott, R. N., Jr., Bandy, B. R. and Rajkumar, A. 2013.** Cenozoic burial metamorphism in eastern Jamaica. *Caribbean Journal of Earth Science*, **46**, 13-30.
- Abbott, R. N., Jr., Jackson, T. A. and McSween, H. Y., Jr. 1996.** Metamorphic conditions in the Westphalia Schists of the Blue Mountain Inlier, Jamaica: Tectonic implications. *International Geology Review*, **38**, 1143-1154.
- Abbott, R. N., Jr., West, D. P., Jr. and Bandy, B. R. 2011.** Thermotectonic history of metamorphic rocks in the Blue Mountain Inlier, Jamaica. *19th Caribbean Geological Conference, Guadeloupe. Program and Abstracts*, 56-57.
- Alexander, E. C., Jr., Michelson, G. M. and Lanphere, M. A. 1978.** MMhb-1: A new ^{40}Ar - ^{39}Ar dating standard, In: **R. E. Zartman (Ed.)**, *Short Papers for the Fourth International Conference on Geochronology, Cosmochronology, Isotope Geology*. U.S. Geological Survey Open-File Report, **78**-701.
- Best, M. G. and Christiansen, E. H. 2001.** *Igneous Petrology*. Blackwell Science, London, 458 pp.
- Cebula, G. T., Kunk, M. J., Mehnert, H. H., Naeser, J. D., Obradovich, J. D. and Sutter, J. F. 1986.** The Fish Canyon Tuff, a potential standard for ^{40}Ar - ^{39}Ar and fission-track dating methods. *Terra Cognita*, *6th International Conference on Geochronology, Cosmochronology and Isotope Geology*. **6**, 139.
- Chubb, L. J. 1954.** The Lazaretto section, Jamaica. *Colonial Geology and Mineral Resources*, **4**, 233-247.
- Dalrymple, G. B., Alexander, E. C., Jr., Lanphere, M. A. and Kracker G. P. 1981.** Irradiation of samples for ^{40}Ar / ^{39}Ar dating using the Geological Survey TRIGA reactor. *U.S. Geological Survey Professional Paper* **1176**, 55 pp.
- Deino, A. L. 2014.** *Users manual for Mass Spec v. 7.961*. *Berkeley Geochronology Center Special Publication*, **3**, 130 pp.
- DeMets, C. and Wiggins-Grandison, M. 2007.** Deformation of Jamaica and motion of the Gonave microplate from GPS and seismic data. *Geophysical Journal International*, **168**, 362-378.
- Dilek, Y. and Furnes, H. 2014.** Ophiolites and their origin. *Elements*, **10**, 93-100.
- Dominguez-Gonzalez, L., Andreani, L., Stanek, K. P. and Gloaguen, R. 2015.** Geomorpho-tectonic evolution of the Jamaican restraining bend. *Geomorphology*, **228**, 320-334.
- Donovan, S. K. 2008.** The 'Forbidden Theory of Mountain Uplift' of Charles Taylor Trechmann (1884-1964): a tectonic theory of the 1950s in context. *Geological Journal*, **43**, 605-619.
- Donovan, S. K. 2010.** Three points of view: Wendall P. Woodring (19891-1983), Charles A. Matley (1866-1947), Charles T. Trechmann (1884-1964), and Jamaican geology in the 1920s and 1930s. In: **S. K. Donovan (Ed.)**, *Jamaican Rock Stars, 1823-1971: The Geologists Who Explored Jamaica*. *Geological Society of America Memoir*, **205**, 59-78.
- Draper, G. 1979.** *Tectonics of the regional metamorphosed rocks of eastern Jamaica*. Ph.D. Dissertation, University of the West Indies, Kingston, Jamaica, 277 pp.
- Draper, G. 1986.** Blueschist and associated rocks in eastern Jamaica and their significance for Cretaceous plate-margin development of the northern Caribbean. *Geological Society of America Bulletin*, **97**, 48-60.
- Draper, G. 1987.** Petrology of the metamorphic rocks of the Blue Mountains, Jamaica. In: **R. Ahmad (Ed.)**, *Proceedings of a Workshop on the Status of Jamaican Geology*. *Geological Society of Jamaica Special Issue*, 120-150.
- Draper, G. 1998.** Geological and tectonic evolution of Jamaica. *Contributions to Geology, University of the West Indies, Mona*, **3**, 3-9.
- Draper, G. 2008.** Some speculations on the Paleogene and Neogene tectonics of Jamaica. *Geological Journal*, **43**, 563-572.
- Fleck, R. J., Sutter, J. F. and Elliot, D. H. 1977.** Interpretation of discordant ^{40}Ar / ^{39}Ar age spectra of Mesozoic tholeiites from Antarctica. *Geochimica et Cosmochimica Acta*, **41**, 15-32.
- Ghiorso, M. S. and Sack, R. O. 1991.** Fe-Ti oxide

- geothermometry: thermodynamic formulation and estimation of intensive variables in silicic magmas. *Contributions to Mineralogy and Petrology*, **108**, 485-510.
- Gradstein, F. M., Ogg, J. G., Schmitz, M. D. and Ogg, G. 2012.** *The Geologic Time Scale 2012*. Elsevier, Boston, 1176 pp.
- Harrison, T. M. and Lovera, O. M. 2013.** The multi-diffusion domain model: past, present and future. In: **F. Jourdan, D. Mark and C. Verati (Eds.),** *⁴⁰Ar/³⁹Ar Dating: From Geochronology to Thermochronology, from Archaeology to Planetary Sciences*. *Geological Society of London Special Publication*, **378**, 91-106.
- Harrison, T. M. and McDougall, I. 1982.** The thermal significance of potassium feldspar K-Ar ages inferred from ⁴⁰Ar/³⁹Ar age spectrum results. *Geochimica et Cosmochimica Acta*, **46**, 1811-1820.
- Hastie, A. R., Kerr, A. C., Mitchell, S. F. and Millar, I. L. 2008.** Geochemistry and petrogenesis of Cretaceous oceanic plateau lavas in eastern Jamaica. *Lithos*, **101**, 323-343.
- Hastie, A. R., Ramsook, R., Mitchell, S. F., Kerr, A. C., Millar, I. C. and Mark, D. F. 2010.** Geochemistry of compositionally distinct Late Cretaceous back-arc basin lavas: Implications for tectonomagmatic evolution of the Caribbean Plate. *Journal of Geology*, **118**, 655-676.
- Hawthorne, F. C., Oberti, R., Harlow, G. E., Maresch, W. V., Martin, R. F., Schumaker, J. C. and Welch, M. D. 2012.** IMA report: Nomenclature of the amphibole supergroup. *American Mineralogist*, **97**, 2031-2048.
- Holland, T. J. B. and Powell, R. 1998.** An internally consistent thermodynamic data set for phases of petrologic interest. *Journal of Metamorphic Geology*, **16**, 309-343.
- Holland, T. J. B. and Powell, R. 2000.** *AX, Mineral activity calculation for thermobarometry*. Cambridge University, Cambridge, computer program AX2 (v. 2.2). web site: <https://www.esc.cam.ac.uk/research/research-groups/holland/ax>
- Hollocher, K. nd.** *Norm 4: norm calculation program*. Web site: http://minerva.union.edu/hollochk/c_petrology/norms.htm
- James-Williamson, S. A., Mitchell, S. F. and Ramsook, R. 2014.** Tectono-stratigraphic development of the Coastal Group of southeastern Jamaica. *Journal of South American Sciences*, **50**, 40-47.
- Kemp, A. W. 1971.** *The geology of the southwest flank of the Blue Mountains*, Jamaica. Ph.D. Discertation, University of the West Indies, Kingston, Jamaica, 307 pp.
- Kretz, R. 1983.** Symbols for rock-forming minerals. *American Mineralogist*, **68**, 277-279.
- Kunk, M. J., Wintsch, R. P., Naeser, C. W., Naeser, N. D., Southworth, C. S., Drake, A. A. and Becker, J. L. 2005.** Contrasting tectonothermal domains and faulting in the Potomac terrane, Virginia-Maryland: Discrimination by ⁴⁰Ar/³⁹Ar and fission-track thermochronology. *Geological Society of American Bulletin*, **117**, 1347-1366.
- Lewis, J. F., Harper, C. T., Kemp, A. W. and Stipp, J. J. 1973.** Potassium-Argon retention ages of some Cretaceous rocks from Jamaica. *Geological Society of America Bulletin*, **84**, 335-340.
- Mann, P. and Burke, K. 1990.** Tranverse intra-arc rifting: Paleogene Wagwater Belt, Jamaica. *Marine and Petroleum Geology*, **7**, 410-427.
- Mann, P., Draper, G. and Burke, K. 1985.** Neotectonics and sedimentation of a strike-slip restraining bend system, Jamaica. In: **K. Biddle (Ed.),** *Strike-slip Deformation, Basin Formation and Sedimentation*. *Society of Economic Paleontologists Special Publication*, **37**, 211-226.
- Mann, P., DeMets, C. and Wiggins-Grandison, M. 2007.** Toward a better understanding of the Late Neogene strike-slip restraining bend in Jamaica: Geodetic, geologic, and seismic constraints. In: **W. D. Cunningham and P. Mann (Eds.),** *Tectonics of Strike-slip Restraining and Releasing Bends*. *Geological Society of London Special Issue*, **290**, 239-253.
- Mann, P., Draper, G. and Burke, K. 1985.** Neotectonics of a strike-slip restraining bend system, Jamaica. In: **K. Biddle and N. Christie-Blick (Eds.),** *Strike-slip deformation, basin formation, and sedimentation*. *SEPM Special Issue*, **37**, 211-226.
- McDougall, I. and Harrison, T. M. 1999.** *Geochronology and thermochronology by the ⁴⁰Ar/³⁹Ar method*. Oxford University Press, New York, Second Edition, 269 pp.
- Mitchell, S. F. 2003.** Sedimentary and tectonic evolution of central Jamaica. In: **C. Bartolini, R. T. Buffler and J. F. Blickwede (Eds.),** *The Circum-Gulf of Mexico and the Caribbean: hydrocarbon habitats, basin formation, and plate tectonics*. *American Association of Petroleum Geologists Memoir*, **79**, 605-623.
- Mitchell, S. F. 2004.** Lithostratigraphy and palaeogeography of the White Limestone Group. In: **S. K. Donovan (Ed.),** *The Mid-Cainozoic White Limestone Group of Jamaica*. *Cainozoic Research*, **3**, 5-29.
- Mitchell, S. F. 2006.** Timing and implications of Late Cretaceous tectonic and sedimentary events in Jamaica. *Geologica Acta*, **4**, 171-178.
- Mitchell, S. F. 2013.** Stratigraphy of the White Limestone of Jamaica. *Bulletin de la Societe Geologique de France*, **184**, 111-118.
- Mitchell, S. F. 2015.** *Geology of the parish of St. Catherine (1:50,000 scale)*. Department of Geography and Geology, University of the West Indies, Mona, Kingston, Jamaica.
- Nier, A. O. 1950.** A redetermination of the relative abundances of the isotopes of Carbon, Nitrogen, Oxygen, Argon, and Potassium. *Physical Review*, **77**, 789.
- Pearce, J. A. 2014.** Immobile element fingerprinting of ophiolites. *Elements*, **10**, 101-108.
- Powell, R. 2005.** THERMOCALC, (v. tc325). web site: <http://www.esc.cam.ac.uk/research/research-groups/holland/thermocalc>
- Powell, R., Holland, T. J. B. and Worley, B. A. 1998.** Calculating phase diagrams involving solutions via on-

- linear equations, with examples using THERMOCALC. *Journal of Metamorphic Geology*, **16**, 577-588.
- Robinson, E. 1967.** Submarine slides in the White Limestone Group, Jamaica. *American Association of Petroleum Geologists Bulletin*, **51**, 569-578.
- Robinson, E. 1994.** Jamaica. In: **S. K. Donovan and T. A. Jackson (Eds.)**, *Caribbean Geology, An Introduction*. The University of the West Indies Publishers Association, Kingston, 111-127.
- Roddick, J. C. 1983.** High precision calibration of $^{40}\text{Ar}/^{39}\text{Ar}$ standards. *Earth and Planetary Science Letters*, **47**, 887-898.
- Sauerzapf, U., Lattard, D., Burchard, M. and Engelmann, R. 2008.** The titanomagnetite-ilmanite equilibrium: New experimental data and thermo-oxybarometric applications to the crystallization of basic and intermediate rocks. *Journal of Petrology*, **49**, 1161-1185.
- Spear, F. S. 1993.** *Metamorphic phase equilibria and pressure-temperature-time paths*. Mineralogical Society of America Monograph, 799 pp.
- Spencer, K. J. and Lindsey, D. H. 1981.** A solution model for coexisting iron-titanium oxides. *American Mineralogist*, **66**, 1189-1201.
- Steiger, R. H. and Jäger, E. 1977.** Subcommittee on geochronology, convention on the use of decay constants in geo- and cosmochronology. *Earth and Planetary Science Letters*, **36**, 359-362.
- Stoener, R. W., Schaeffer, O. E. and Katcoff, S. 1965.** Half-lives of Argon-37, Argon-39, and Argon-42. *Science*, **148**, 1325-1328.
- Sun, S. S. and McDonough, W. F., 1989.** Chemical and isotopic systematics of oceanic basalts, implications for mantle composition and processes. *Geological Society of London Special Paper*, **42**, 313-345.
- Villa, I. M. 2013.** Diffusion of Ar in K-feldspar: Present and absent. In: **F. Jourdan, D. Mark and C. Verati (Eds.)**, $^{40}\text{Ar}/^{39}\text{Ar}$ Dating: From Geochronology to Thermochronology, from Archaeology to Planetary Sciences. *Geological Society of London Special Publication*, **378**, 107-116.
- Weast, R. C. (Ed.) 1981.** *Handbook of Chemistry and Physics*, 62nd Edition. CRC press, Boca Raton, FL, 1700 pp.
- West, D. P., Jr., Abbott, R. N., Jr., Bandy, B. R. and Kunk, M. J. 2014.** Protolith provenance and thermotectonic history of metamorphic rocks in eastern Jamaica: Evolution of a transform plate boundary. *Geological Society of America Bulletin*, **126**, 600-614.
- Whitney, D. L. and Evans, B. W. 2010.** Abbreviations for names of rock-forming minerals. *American Mineralogist*, **95**, 185-187.
- Wiewiora, A. and Weiss, Z. 1990.** Crystallochemical classification of phyllosilicates based on the unified system of projection of chemical composition: II. The chlorite group. *Clay Minerals*, **25**, 83-92.
- Willner, G., Willner, A. P., Maresch, W. V. and Schreyer, W. 1995.** Pressure-temperature evolution of low-grade alkali-amphibole-bearing assemblages of the Mt. Hibernia schist, Blue Mountains, Jamaica. In: *14th Caribbean Geological Conference Program with Abstracts. Port-of-Spain, Trinidad and Tobago*, Geological Society of Trinidad, 86 pp.

Editorial Responsibility: Sherene James-Williamson. Type setting: Simon F. Mitchell

Accepted 20th March 2016